Available online at www.sciencedirect.com
SCIENCE DIRECT®
Journal of Sound and Vibration 290 (2006) 242–263
JOURNAL OF SOUND AND VIBRATION
www.elsevier.com/locate/jsvi

Experimental investigation of seismic damage identification using PCA-compressed frequency response functions and neural networks

Y.Q. Ni*, X.T. Zhou, J.M. Ko

Department of Civil and Structural Engineering, The Hong Kong Polytechnic University, Hung Hom, Kowloon, Hong Kong

Received 1 July 2003; received in revised form 23 March 2005; accepted 29 March 2005
Available online 15 June 2005

Abstract

This paper presents an experimental investigation of seismic damage identification of a 38-storey tall building model using measured frequency response functions (FRFs) and neural networks (NNs). The 1:20 scale reinforced concrete structure is tested on a shaking table by exerting successively enhanced ground earthquake excitation to generate trifling, moderate, serious and complete (nearly collapsed) damage, respectively. After incurring the earthquake excitations at each level, a 20-min white-noise random excitation of low intensity is applied to the structure to produce ambient vibration response, from which FRFs are measured for post-earthquake damage detection by means of the NN technology. Principal component analysis (PCA) is pursued to the measured FRFs for dimensionality reduction and noise elimination, and then the PCA-compressed FRF data are used as input to NNs for damage identification. After a study on tolerance of PCA-reconstructed FRFs to measurement noise, different PCA configurations are designed for overall damage evaluation and damage location (distribution) identification, respectively. It is shown that the identification results by means of the FRF projections on a few principal components are much better than those directly using the measured FRF data, and agree fairly well with the visual inspection results of seismic damage during tests.

*Corresponding author. Tel.: +852 2766 6004; fax: +852 2334 6389.
E-mail addresses: ceyqni@polyu.edu.hk (Y.Q. Ni), 00900376r@polyu.edu.hk (X.T. Zhou), cejmko@polyu.edu.hk (J.M. Ko).
URL: http://www.cse.polyu.edu.hk/~dynamics.

0022-460X/$ - see front matter © 2005 Elsevier Ltd. All rights reserved.
doi:10.1016/j.jsv.2005.03.016

1. Introduction

Civil engineering structures deteriorate with time and continuously accumulate damage during their service life due to natural hazards such as earthquake, storm, fire, long-term fatigue and corrosion. Many efforts have been made on health monitoring and damage assessment of civil infrastructure for avoiding catastrophic structural failure and making proper decision on repair, partial replacement or demolition. Among others, the vibration-based damage identification technique has attracted significant interest for researchers and engineers in the past two decades [1,2]. This approach usually uses measured change in natural frequencies and modal shapes to evaluate change in physical properties that may indicate structural damage or degradation. Also, vibration-based damage detection using measured frequency response functions (FRFs) has been studied by a number of researchers [3–9]. As modal parameters (natural frequency, mode shape and modal damping) are indirectly-measured test data, they could be contaminated by measurement error as well as modal extraction error, and provide less information than FRF data. In this sense, it is more reasonable and reliable to use directly-measured FRF data for structural damage detection, particularly for structures with closely spaced modes. However, identification accuracy of the FRF-based damage detection method depends heavily on the selected frequency range. If improper frequency points are adopted, the measurement error may seriously affect the identification results. Using the FRF data in the vicinity of resonant frequencies is not necessary to provide the most reliable damage detection [10].

Neural networks (NNs) have been a promising computation tool for damage identification due to their strong capabilities in pattern recognition and classification, data interpretation, function approximation, etc. The combined use of FRFs with NNs for structural damage detection was reported in the literature. For example, Wu et al. [11] studied the damage detection of a three-storey frame by using selected frequency points of response spectrum as input to a neural network; Chaudhry and Ganino [12] used frequency response data over a specified frequency range to train a neural network for delamination identification in a beam structure; Manning [13] trained a neural network using active member transfer function information to classify damage and predict damage extent; Rhim and Lee [14] addressed damage detection using a neural network with input data being transfer functions of auto-regressive model; Luo and Hanagud [15] used FRF data obtained from PVDF sensors to train a neural network for delamination detection; Chang et al. [16] constructed a signal anomaly index vector in terms of FRF data before and after damage as input to a neural network for bridge damage detection. However, a bottleneck remaining for the use of FRFs with NNs is the huge size of FRF data. Direct use of full-size FRF data will lead to the neural network having a large number of input nodes, which cause the problem of training convergency and computational efficiency. If only using partial FRF data, improper selection of data points from frequency windows may result in the loss of important information. In order to circumvent the above difficulty, Zang and Imregun [17,18] recently proposed a novel approach to compress FRF data by principal component analysis (PCA) within the framework of damage detection. They obtained size-reduced projections of measured FRF data on significant principal components and used such compressed FRFs as neural network input for structural damage detection.

This paper describes an experimental study to compare the identification accuracy of the combined FRF and NN technique with and without PCA pre-processing when applied to seismic damage

detection of high-rise building structures. A 1:20 scale model of a 38-storey residential building is tested on a shaking table to subject to four levels of earthquake including minor earthquake, moderate earthquake, strong earthquake and super-strong earthquake. Accordingly, the structure suffers from trifling, moderate, serious and complete (nearly collapsed) damage, respectively. After the earthquake excitations at each level, white-noise random excitation is applied to the structure to imitate ambient vibration, and excitation accelerations at the base plate as well as response accelerations at nine floors of the structure under the ambient vibration are measured for the purpose of damage detection. FRFs of the structure are obtained in the healthy state and at different damage levels. PCA is applied to the measured FRFs to find the principal components and to determine a proper number of truncated significant components through comparing the reconstructed FRFs with the original ones. The noise tolerance of the reconstructed FRFs using a few principal components is studied by introducing additional artificial noise in the time-domain records of excitation and response. Different PCA configurations are formulated as input to neural networks for overall damage evaluation and damage location (distribution) identification, respectively. Identification results using the PCA projections as input to neural networks are also compared with those obtained by directly using the measured FRF data as input to neural networks.

2. Theoretical background

2.1. Dimensionality reduction of FRFs using PCA

PCA is a statistical technique that linearly transforms an original set of variables into a substantially smaller set of uncorrelated variables that represents most of the information in the original set of variables [19,20]. It can be viewed as a classical method of multivariate statistical analysis for achieving a dimensionality reduction. Because of the fact that a small set of uncorrelated variables is much easier to understand and use in further analysis than a larger set of correlated variables, this data compression technique has been widely applied to virtually every substantive area including engineering, biology, medicine, chemistry, meteorology, geology, as well as the behavioral and social sciences.

Using an orthogonal projection, the original set of variables in an N-dimensional space is transformed into a new set of uncorrelated variables, the so-called principal components (PCs), in a P-dimensional space such that $P<N$. In other words, it seeks to project the high-dimensional data into a new low-dimensional set of Cartesian coordinates $(z_1, z_2, \ldots, z_P)$. The new coordinates have the following property: z_1 is the linear combination of the original coordinates x_i $(i = 1, 2, \ldots, N)$ with maximal variance, z_2 is the linear combination which explains most of the remaining variance and so on. If exist P-coordinates which are actually a linear combination of N $(>P)$ variables, then the first P principal components will completely characterize the data and the remaining $N-P$ will be zero. The calculation is described as follows. Given the measurement data sets $\{x\}_j = \{x_{j1}, x_{j2}, \ldots, x_{jN}\}^{\mathrm{T}}$ $(j = 1, 2, \ldots, M)$, where T denotes transposition and M is the total number of measurements, we form the $N \times N$-dimension covariance matrix $[C]$ as

$$[C] = \sum_{j=1}^{M} \{x\}_j \{x\}_j^{\mathrm{T}} \tag{1}$$

and perform singular value decomposition of $[C]$ as

$$[C] = [A][\Lambda][A]^{\mathrm{T}}, \tag{2}$$

where $[\Lambda]$ is a diagonal matrix. The transformation to principal components is then accomplished as

$$\{z\}_j = [A]^{\mathrm{T}}(\{x\}_j - \{\bar{x}\}), \tag{3}$$

where $\{\bar{x}\}$ is the vector of means of the x-data. From the point of view of dimensionality reduction, PCA works by discarding those linear combinations of the data which contribute least to the overall variance or range of the data set.

In the present study, PCA is used to reduce the dimensionality of measured FRF data. With the measured FRF vectors $\{x\}_j$ $(j = 1, 2, \ldots, M)$, it is easy to calculate the principal component matrix $[A]$ and their transformations $\{z\}_j$ $(j = 1, 2, \ldots, M)$ by using the above formulae. In order to determine how many principal components are enough for reserving most information of the original FRF data, FRF reconstruction using only a few principal components will be conducted firstly. The projection of the original frequency response function matrix $[H(\omega)]_{M\times N}$ which consists of M FRFs and has N frequency points for each FRF, on the N principal components, is given by [17,18]

$$[B]_{M\times N} = [H(\omega)]_{M\times N}[A]_{N\times N}. \tag{4}$$

The projection matrix $[B]$ and the principal component matrix $[A]$ can be portioned into two sub-matrices with P significant principal components and $(N-P)$ insignificant principal components (which actually are trivial and thus not really principal) as

$$[B]_{M\times N} = [[B_1]_{M\times P} \vdots [B_2]_{M\times(N-P)}], \tag{5a}$$

$$[A]_{N\times N} = [[A_1]_{N\times P} \vdots [A_2]_{N\times(N-P)}]. \tag{5b}$$

The frequency response function matrix can therefore be reconstructed for only P principal components as

$$\begin{aligned}[H_R] &= [B][A]^{\mathrm{T}} \\ &= [[B_1]_{M\times P} \vdots [B_2]_{M\times(N-P)}][[A_1]_{N\times P} \vdots [A_2]_{N\times(N-P)}]^{\mathrm{T}} \\ &\cong [B_1]_{M\times P}[A_1]^{\mathrm{T}}_{P\times N}. \end{aligned} \tag{6}$$

In addition to using different number of principal components for reconstructing FRFs, the reconstruction of FRFs will also be carried out under a variety of noise levels to examine the noise tolerance of PCA-compressed FRFs. Noise corruption in the original measured FRFs is attained by adding the time-domain excitation and response signals independently with random variable sequences of normal distribution.

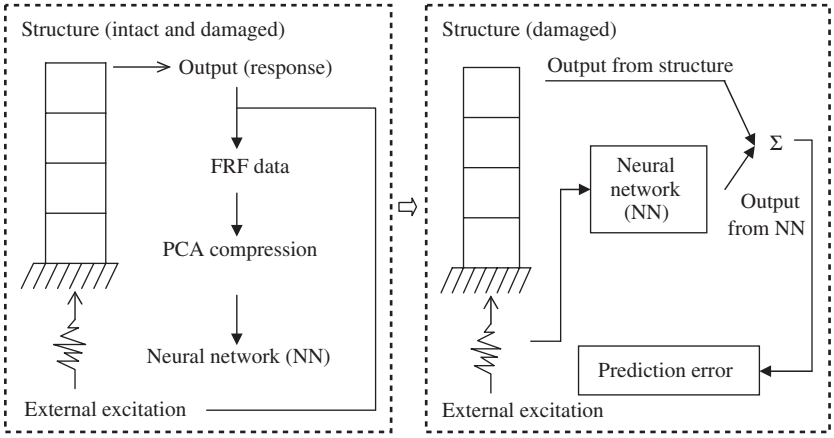

Fig. 1. Illustration of damage identification using NN.

2.2. Damage detection using NN

Implementing the neural network technique for structural damage detection includes two stages: the training stage and the detection stage, as shown in Fig. 1. When FRFs are used with NNs for damage identification, the FRFs data of a structure in intact state and under a series of given damage scenarios, obtained analytically or experimentally, are used as training samples to train the neural network. The trained neural network is able to predict the damage state when a new set of measured FRF data is presented as input to the trained network. However, direct use of full-size FRF data will result in huge configuration of the network input layer which brings about the problem of iteration divergency in training and computational inefficiency. In the present study, the FRF projections on a small number of principal components obtained by PCA are instead taken as input to neural networks for seismic damage detection of the tested structure. As shown in Fig. 2, a three-layer feed-forward network with the Sigmoid activation function and back-propagation algorithm is herein employed for this purpose. The configured network has only one output node. When a set of FRF projections obtained from a structural region is fed as testing samples into the network, its output indicates the damage severity at this specific region.

3. Shaking table tests

3.1. Experimental description

The tested structure, as shown in Fig. 3, is a 1:20 scale model of a typical high-rise residential building in Hong Kong with the transfer plate system and large open-space at the lower stories. The prototype building is a 38-storey reinforced concrete structure with 34 stories typical floors supported by a transfer plate and a three-level podium. The scaled model, which is 2.370 m long, 2.160 m wide and 6.515 m high, is constructed with Nos. 1–3 bottom floors, one transfer plate, Nos. 4–38 typical floors, and Nos. 39–42 top machine floors. In the model structure, sizes of the

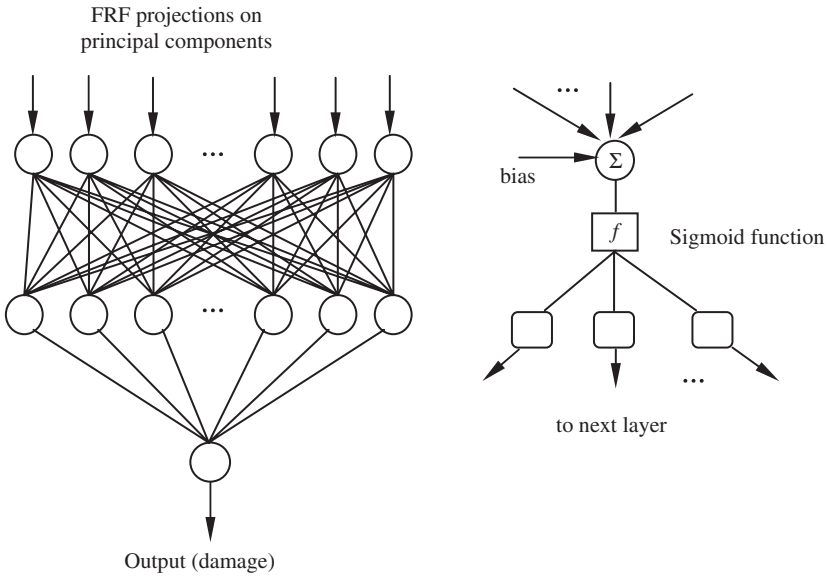

Fig. 2. Neural network topology and connection at a typical node.

concrete beams, columns, slabs and shear walls and core walls are strictly fabricated following the dimensional scale ratio 1:20, and the structural materials (including additional masses and reinforcements) are selected according to the similitude law. The section area and number of reinforcements are designed to meet the requirement of the reinforcement ratio used in the prototype building.

The model structure was tested on a $5\,m \times 5\,m$, 6-dof shaking table by exerting successively enhanced earthquake waves (minor earthquake, moderate earthquake, strong earthquake and super-strong earthquake excitations under rock, medium soil and soft soil site conditions). Accordingly, it was subjected to seismic destroy extending from trifling, moderate, serious damage till to complete (nearly collapsed) damage. These shaking table tests conducted in consecutive stages with increasing magnitude of earthquake excitation are mainly for the purpose of evaluating seismic performance of tall buildings in Hong Kong [21]. Fig. 4 shows the visual inspection results of damage of the structure after experiencing four levels of earthquake excitations. When the structure was subjected to minor earthquake excitations, fine 'hair-line' cracks were found in several structural members at the podium level (transfer plate). These cracks were barely noticeable and the crackwidths were very small. When subjected to moderate earthquake excitations, cracks previously appeared under minor earthquake excitation propagated with slight increase in crackwidth. More importantly, new horizontal and diagonal cracks were found between floors Nos. 4 and 8 above the transfer plate, indicating the shift of structural damage to the stories above podium level. Under strong earthquake excitations, besides increase in the crackwidths and propagation of the cracks found in moderate earthquake excitations, more than 50 new cracks were found. Most of them appeared at stories above the transfer plate and at the middle and upper stories. For example, cracks were found on the wall and the central core at floors Nos. 8–10, and a penetrated horizontal crack was found on the wall

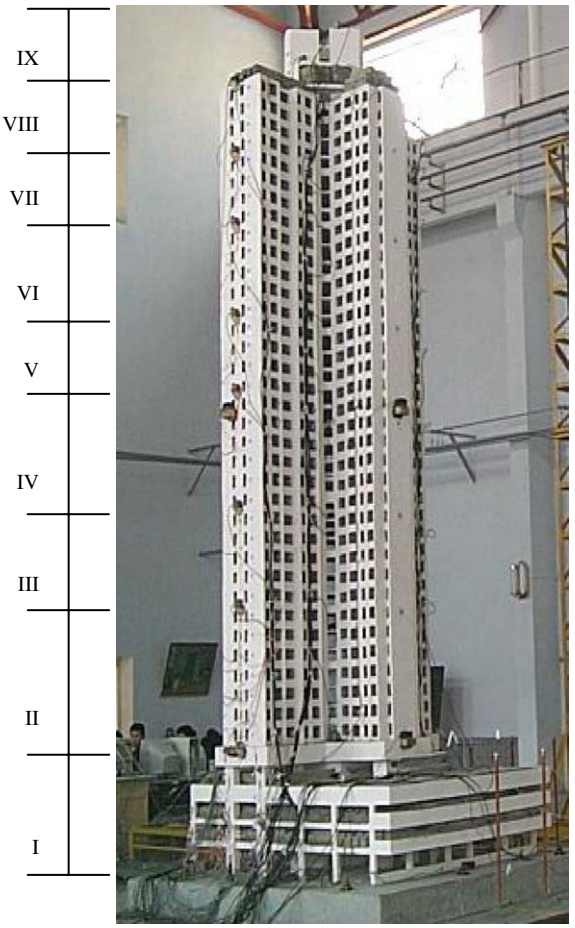

Fig. 3. Tested tall building model.

at floor No. 35. When subjected to super-strong earthquake excitations, integrity of the structure was destroyed. The failure is mainly due to complete separation of an end shear wall at the vicinity above the transfer plate. Horizontal cracks appeared on the surfaces of the floor slabs in all the stories, with the severest cases at floors Nos. 4–10.

After experiencing each level of earthquake excitations, the structure was subjected to white-noise random excitation of low intensity at its base to generate ambient vibration, and the excitation and response under the ambient vibration were measured for structural damage identification. A total of 27 accelerometers are distributed uniformly along the height to track the ambient vibration response at south–north direction (direction-X) and east–west direction (direction-Y). In order to facilitate damage location, the structure is divided into nine regions along the elevation as shown in Fig. 3, each consisting of 4–5 floors. For each region, three accelerometers are installed at one floor, respectively, at the west and east sides of floor plan in direction-X and at the centre of floor plan in direction-Y. The 20-min white-noise random

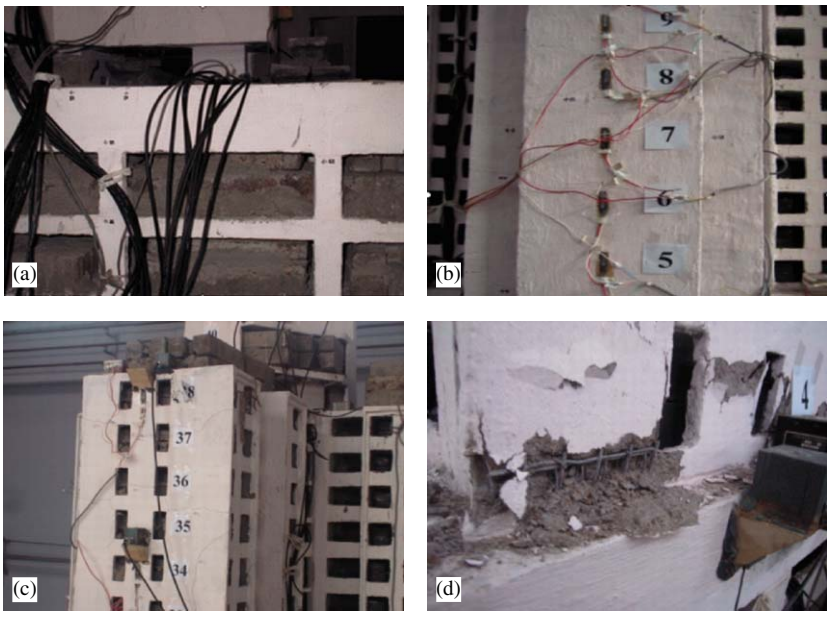

Fig. 4. Visual inspection of damage after four levels of earthquake excitations: (a) minor earthquake; (b) moderate earthquake; (c) strong earthquake; (d) super-strong earthquake.

excitation after each level of earthquake excitations was exerted in terms of six time segments, each lasting about 3 min. Because the level of the white-noise random excitation is considerably low, it is regarded that the structure holds the same damage state during the six time segments. The excitation and response accelerations during the ambient vibration were measured with a sampling rate of 100 Hz. Only the excitation and response records in direction-X are used in the present study. Table 1 shows the sequence of the shaking table tests, including both earthquake excitations (for seismic performance evaluation) and white-noise random excitations (for damage detection), where 'bi-direction' implies simultaneous excitation of earthquake in directions-X and Y. Stories with obviously observed cracks after each level of earthquake excitations are also indicated in the table. It should be noted that several earthquake excitations (different site conditions and different attack directions) have been exerted for each level, after which the 20-min ambient vibration testing is conducted.

3.2. Measured FRFs

FRFs of the structure in healthy and damage states are obtained by low-intensity white-noise random excitations. As mentioned earlier, each 20-min random excitation consists of six time segments. One segment, which lasts more than 3 min, contains more than $3 \times 60 \times 100 = 18{,}000$ sampling data in the time domain with the sampling rate of 100 Hz. The FRFs are obtained with the basic FFT length of 1024 points and the FFT average number of 1000. As a result, each FRF contains 512 spectral lines. Six FRFs corresponding to the six time segments are obtained for the

Table 1
Sequence of shaking table tests and observation of cracked stories

No.	Damage cases (cracked stories)	Excitation type	Descriptions
1	No damage	Modal test	(a) Without artificial mass attached
2			(b) With artificial mass attached
3		White noise	20-min white noise excitation
4	Trifling damage (transfer plate & C04)	Minor earthquake excitations	(a) Bi-direction on hard soil site
5			(b) Bi-direction on moderate soft soil site
6			(c) Bi-direction on soft soil site
7			(d) Direction-X on hard soil site
8			(e) Direction-Y on hard soil site
9			(f) Direction-X on moderate soft soil site
10			(g) Direction-Y on moderate soft soil site
11			(h) Direction-X on soft soil site
12			(i) Direction-Y on soft soil site
13		Modal test	After minor earthquake excitations
14		White noise	20-min white noise excitation
15	Moderate damage (C04, C07 & C08)	Moderate earthquake excitations	(a) Bi-direction on hard soil site
16			(b) Bi-direction on moderate soft soil site
17			(c) Bi-direction on soft soil site
18			(d) Direction-X on hard soil site
19			(e) Direction-Y on hard soil site
20		Modal test	After moderate earthquake excitations
21		White noise	20-min white noise excitation
22	Serious damage (C04, C07, C08, C10, C25, C30 & C34)	Strong earthquake excitations	(a) Direction-X on hard soil site
23			(b) Direction-X on moderate soft soil site
24			(c) Direction-X on soft soil site
25		Modal test	After strong earthquake excitations
26		White noise	20-min white noise excitation
27	Complete damage (C04, C07, C08, C10, C15, C25, C30, C34 & C39)	Super-strong earthquake excitations	(a) Direction-X on hard soil site
28			(b) Direction-X on moderate soft soil site
29			(c) Direction-X on soft soil site
30		Modal test	After super-strong earthquake excitations
31		White noise	20-min white noise excitation

healthy state and for each damage state. Fig. 5 shows the measured FRFs of the structure in healthy and different damage states, which are generated using the response at floor No. 38 in direction-X subject to the base excitation in the same direction. It is seen that the damage not only changes the resonant frequency, but also makes a reduction of the resonant peak.

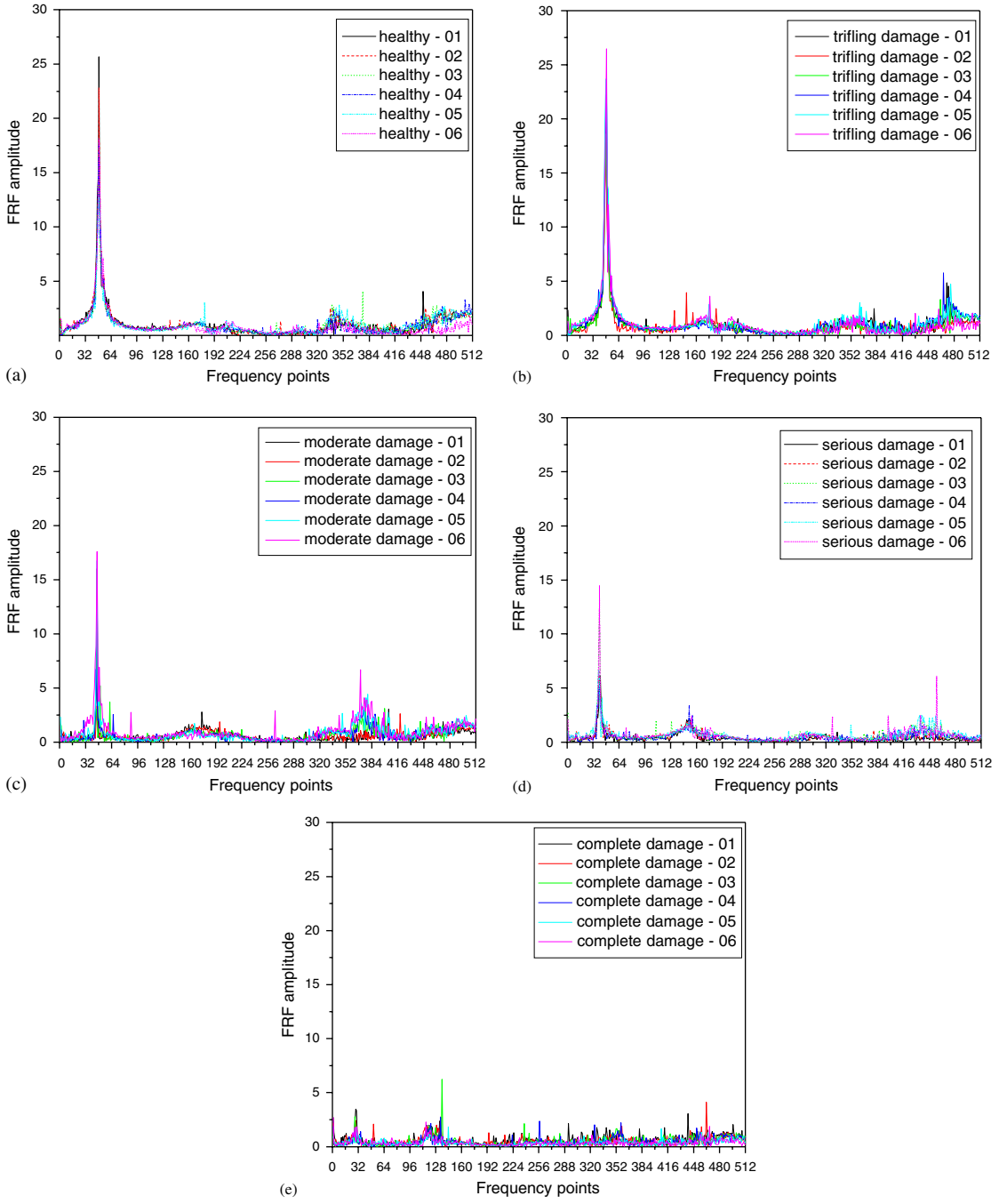

Fig. 5. FRFs of healthy and damaged structure from measurement at floor No. 38: (a) healthy; (b) trifling damage; (c) moderate damage; (d) serious damage; (e) complete damage.

4. Compression of FRFs using PCA

4.1. Selection of principal components

The present study uses FRF information as input to NNs for structural damage detection. Because the size of the FRF data (9×3 measurement points, six segments for each case, and 512 spectral lines in each FRF) is prohibitive for a direct use, PCA is applied as a pre-processing to reduce the data dimensionality. The most significant principal components obtained from FRFs contain those features which are dominant in most of the frequency responses. In order to determine an appropriate number of principal components which can represent the original FRFs well, the reconstruction using a different number of principal components are investigated. Firstly, a total of five FRF matrixes corresponding to no damage, trifling damage, moderate damage, serious damage and complete damage cases are generated, where each matrix has six rows consisting of FRFs from the six measurement segments and 512 columns equal to the number of spectral lines in each FRF. Then, by combining the above five matrices, we yield a 30×512 matrix consisting of 30 FRFs which represent both healthy structure and four damage cases. Subsequently, with the use of Eqs. (1)–(6), the principal components are calculated and FRFs are reconstructed using 5, 13 and 30 principal components, respectively, as shown in Figs. 6–8.

It should be noted that both the original FRFs and reconstructed ones plotted in the above figures are average of the six FRFs for each healthy or damage case. When only five principal components are used, the FRFs cannot be reconstructed well. Reconstructed FRFs by 13 principal components can represent the original FRFs well as a whole. When using 30 principal components, the reconstructed FRFs are almost identical with the original ones. In conclusion, the more principal components used, the better FRF reconstruction. Considering that 13 principal components are enough to account for most of features in the original FRF data, we use these principal components for the subsequent noise-tolerance investigation and seismic damage identification.

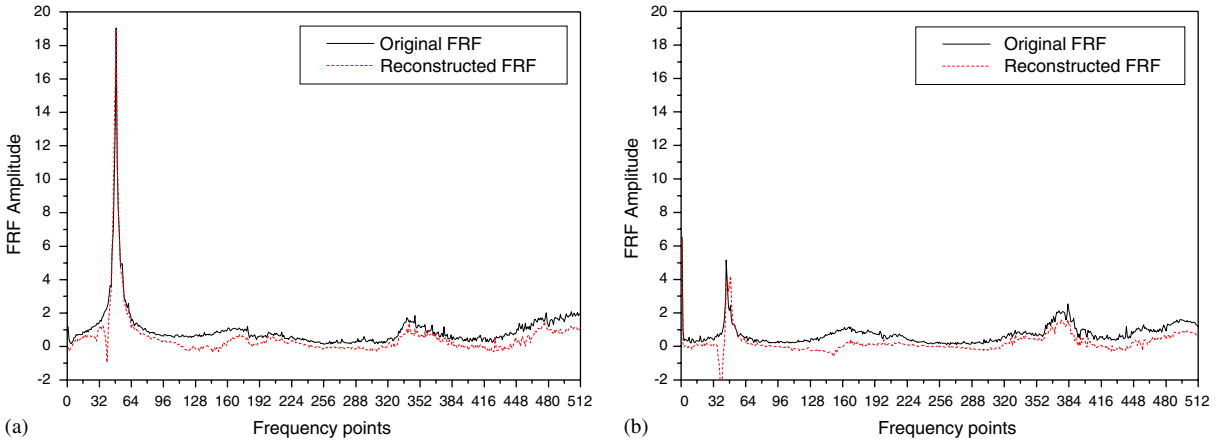

Fig. 6. Original and reconstructed FRFs using five principal components: (a) healthy; (b) moderate damage.

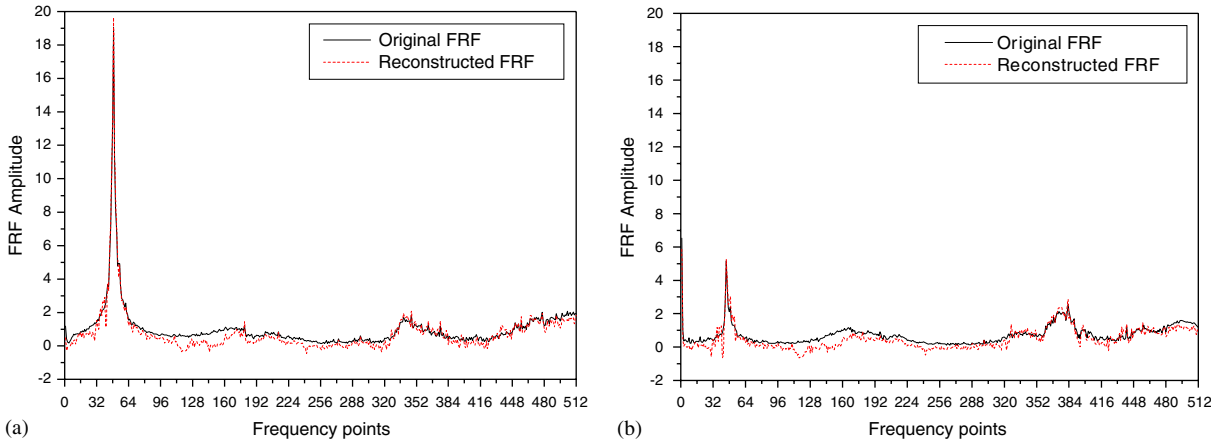

Fig. 7. Original and reconstructed FRFs using 13 principal components: (a) healthy; (b) moderate damage.

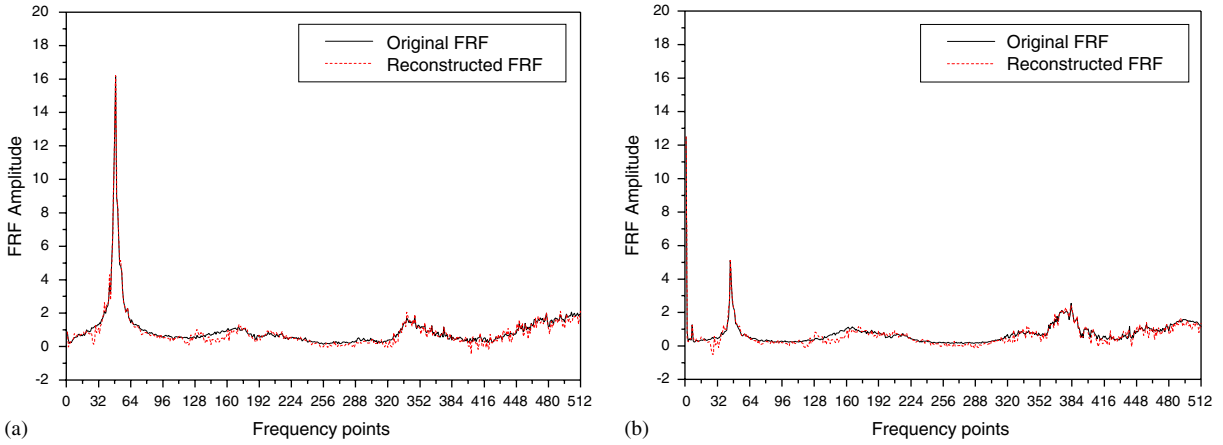

Fig. 8. Original and reconstructed FRFs using 30 principal components: (a) healthy; (b) moderate damage.

4.2. Tolerance to measurement noise

As opposed to the most significant principal components containing dominant features, measurement noise corrupted in excitation and response signals will be represented by the less significant components. In other words, reconstructing the frequency response by using only a limited number of principal components should perform data compression as well as remove the majority of noise. In order to study the noise-tolerant property of PCA, a set of normally distributed random sequences with zero mean and σ standard deviation are added to the original time-domain excitation and response records directly, to simulate additional measurement noise. Let $x(t)$ denote the original time-domain signal and $r(\sigma)$ a sequence of man-made random noise,

the noise-corrupted 'measurement' is obtained as

$$\bar{x}(t) = x(t) + r(\sigma), \tag{7}$$

where the standard deviation σ is herein taken as 0.01 and 0.05 to represent low and high noise level, respectively. The excitation and response signals are corrupted with the noise samples independently.

Figs. 9 and 10 illustrate the original and reconstructed FRFs of the healthy structure at floor No. 38 in low and high noise levels, respectively. The reconstructed FRFs are obtained using the first 13 principal components. For each noise level, random sequences are added independently to the measured excitation and response to produce 30 FRFs corrupted with man-made noise as

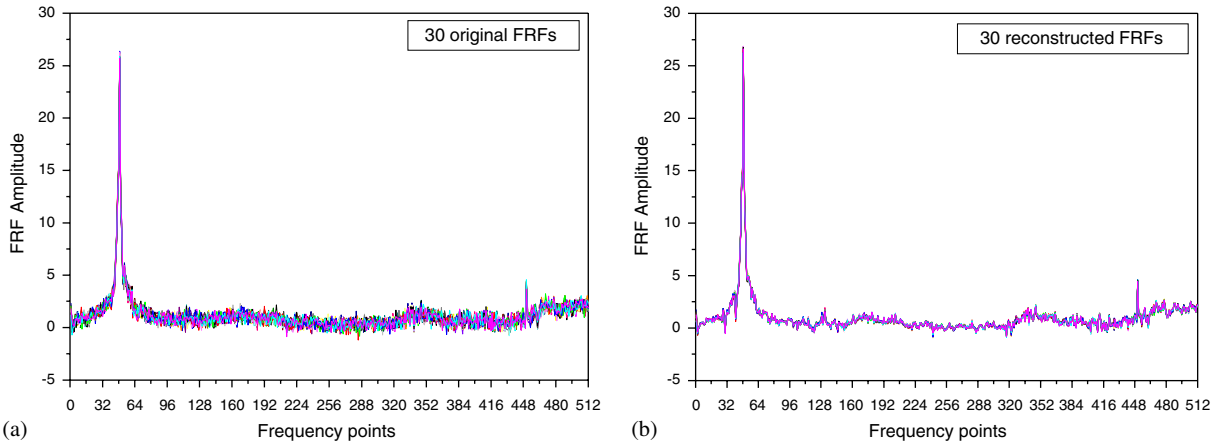

Fig. 9. Original and reconstructed FRFs in low noise level ($\sigma = 0.01$): (a) original FRFs; (b) reconstructed FRFs.

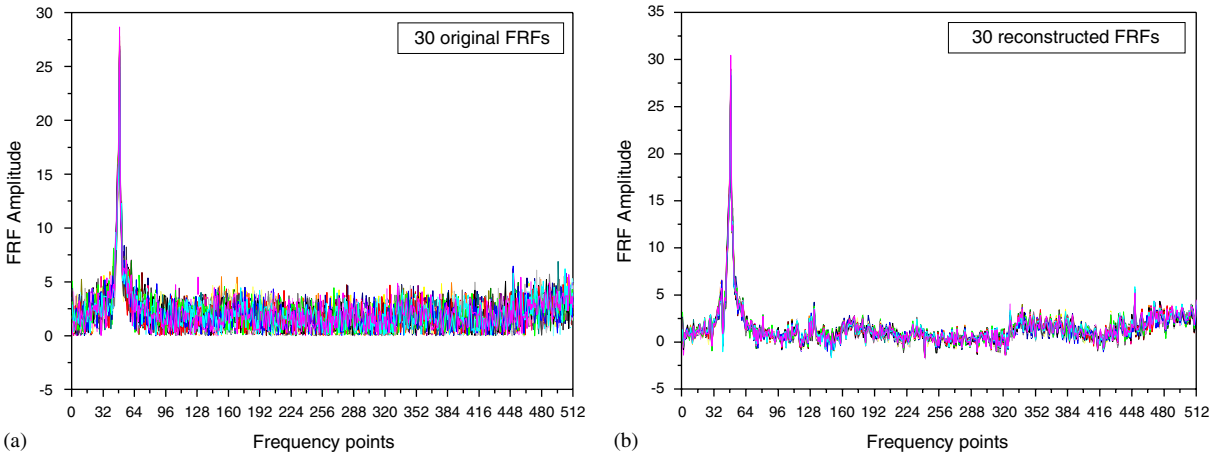

Fig. 10. Original and reconstructed FRFs in high noise level ($\sigma = 0.05$): (a) original FRFs; (b) reconstructed FRFs.

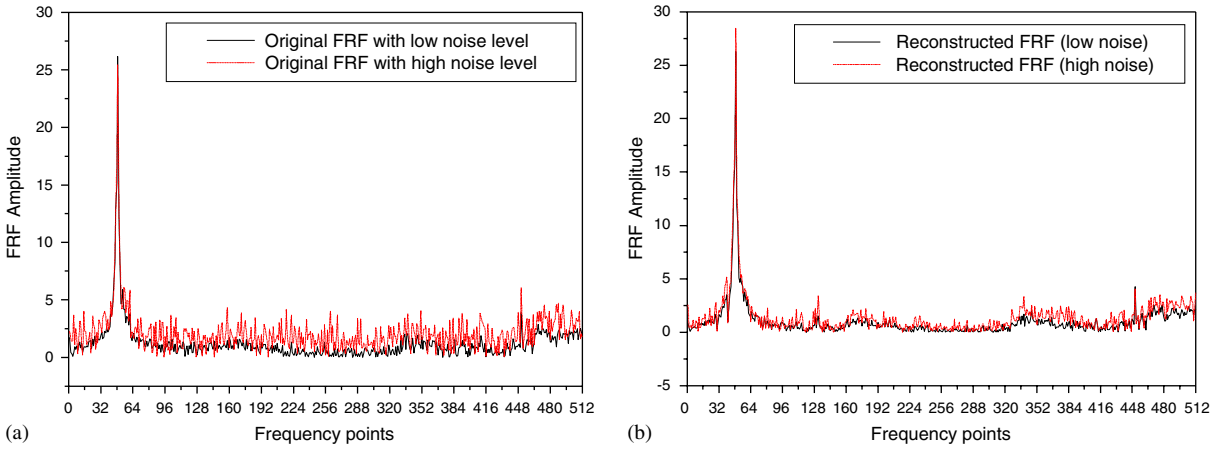

Fig. 11. Comparison of FRFs obtained under different noise levels: (a) original FRFs; (b) reconstructed FRFs.

shown in the figures. In the low noise case, the original FRFs have considerable fluctuation due to the noise, whereas the reconstructed ones have much smaller fluctuation. The 13 principal components retain prevailing features of the origin FRFs while discarding the trivial variation caused by noise. When the high level noise is introduced, fluctuations of both the original FRFs and reconstructed ones become more significant than those in the low noise corruption case. The fluctuation is so large as to mask the variation of the original FRFs with frequency. Nevertheless, the reconstructed FRFs in this noise level represent the variation detail favourably and are quite consistent with each other. It means that PCA is eligible for filtering unwanted measurement noise. In Fig. 11, two original FRFs corresponding to the low and high noise levels are plotted in the same diagram, which is also the case for reconstructed FRFs. It is seen that the original FRFs vary significantly with the increase of noise level, whereas the reconstructed ones keep a high consistency, even in the high frequency range. This observation attests again that PCA is capable of reducing the dimensionality of the original FRF sets with reserving most of the information and highly tolerant to measurement noise. Thereafter, PCA-compressed FRF projections will be used as input to NNs for seismic damage identification of the tested structure.

5. Damage identification using NNs

5.1. Overall damage assessment

Damage identification of the tested structure includes overall seismic damage assessment and damage location (distribution) evaluation. For overall damage assessment, three neural network input configurations are designed for comparative study. The first scheme is to use 13 and 30 directly measured FRF points around the first resonant frequency (4.68 Hz) as network input, respectively. Apparently in this scheme only partial information over a specified frequency range rather than all information on the whole FRF is utilized. In the second scheme, a few principal

component projections of FRFs measured at one specific floor are taken as network input. Here, we adopt 13 principal components of FRF obtained from floor No. 38. The third scheme for overall damage assessment is to utilize the complete information of FRFs obtained from all nine measurement points at floor Nos. 4, 10, 15, 21, 25, 30, 34, 38 and 42. Based on 13 principal components extracted from each measurement point, a total of $13 \times 9 = 117$ principal component projections are grouped together, which contain the information of nine FRFs and spatial configuration. However, an input vector consisting of 117 elements seems still too burdensome for network training. A twofold-PCA strategy is thus proposed. PCA is executed again on the obtained 117 principal component projections, and 30 principal component projections obtained from the second PCA are used as network input. For distinction, the three schemes are referred to as direct FRF method, once-PCA method and twofold-PCA method, respectively. In all the three schemes, the three-layer feed-forward network is configured to have 15 nodes in the hidden layer and one output node indicating overall damage severity.

The training samples of neural networks are usually obtained by numerical simulations using an analytical or finite-element model of the structure [11] or directly obtained from model experiments [22]. In order to obtain analytically generated training samples for the present study, finite-element models of both the healthy structure and the earthquake-damaged structure are needed. However, it is found that for the tested tall building model it is extremely difficult to establish finite-element models of the earthquake-damaged structure after experiencing various levels of earthquake excitations, due to the lack of appropriate representation of cracking and ductility performance. So we have no alternative but to use experimental data as training samples of the neural networks. As mentioned earlier, six ambient vibration measurement segments have been obtained after the structure experiences each level of earthquake excitations. Data of the first three segments are used herein to train the neural networks, while data of the second three segments are used for damage evaluation. Because the ambient vibration data were obtained after the structure experienced several earthquake events at each level, the training samples can be understood corresponding to several damage states rather than one damage state. However, such obtained training samples are still limited and may be not enough for learning all damage patterns. It also results in the testing samples for damage evaluation exercise being not significantly different from the training samples in the sense that they are experimentally derived under identical damage states. As a result, good performance for such testing samples does not necessarily indicate good generalization capability of the trained neural networks. But the damage evaluation results still provide a good experimental validation and performance comparison of using PCA-compressed FRF data and directly using measured FRF data as input to neural networks for damage identification, respectively.

In order to study identification accuracy under different noise levels, all the measurement signals are additionally corrupted by artificial random noise sequences with $\sigma = 0.01$ and $\sigma = 0.05$, respectively. For each noise level, 100 sample sets of time-domain excitation and response signals are produced by adding the first three measurement segments with random sequences for neural network training, and another 100 sample sets are independently generated from the second three measurement segments for damage evaluation use. There is no overlap between the 100 training samples and the 100 testing samples. To quantitatively define damage extents for the five cases, the target output in neural network training phase is specified as

Table 2
Neural network target output and permitted actual output for damage evaluation

Damage cases	Specified target output	Permitted actual output
No damage (N)	0.1	<0.2
Trifling damage (T)	0.3	0.2–0.4
Moderate damage (M)	0.5	0.4–0.6
Serious damage (S)	0.7	0.6–0.8
Complete damage (C)	0.9	>0.8

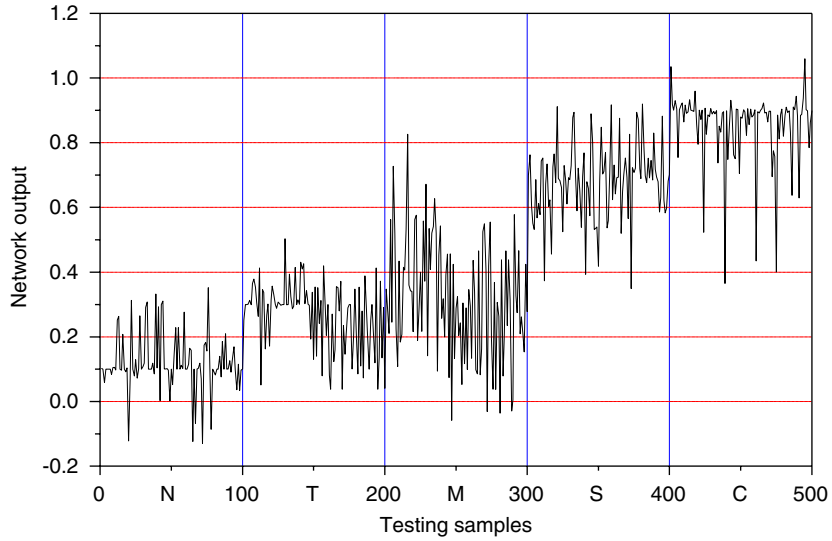

Fig. 12. Identification results by direct FRF method (30 FRF points, $\sigma = 0.05$).

a definite value, whereas the actual output in testing (damage detection) phase is defined as a permitted range, as shown in Table 2. If and only if the network output for a testing sample lies in the permitted range corresponding to the respective damage case, we count that testing sample as correct identification.

Figs. 12–14 show the predicted output by neural networks using the three schemes, where N, T, M, S and C denote testing samples of no damage, trifling damage, moderate damage, serious damage and complete damage cases, respectively. The damage severity is correctly predicted when the neural network output is within the permitted range of the corresponding damage level. It is observed that the damage evaluation results by twofold-PCA method are the best and the results by direct FRF method are the worst. Table 3 gives the correct identification times out of 500 testing samples and the identification accuracy (IA), which is defined as the ratio of the number of correct identification times to the total number of testing samples. It is found that when using

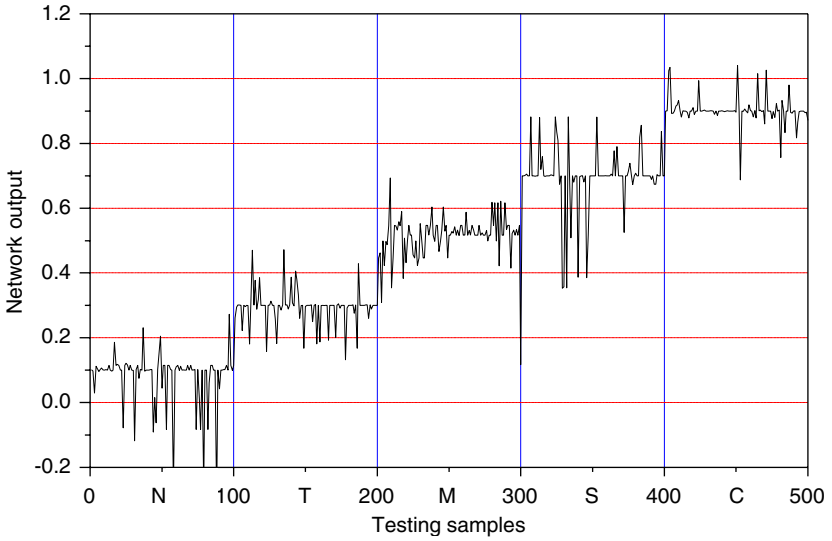

Fig. 13. Identification results by once-PCA method (13 PCs, $\sigma = 0.05$).

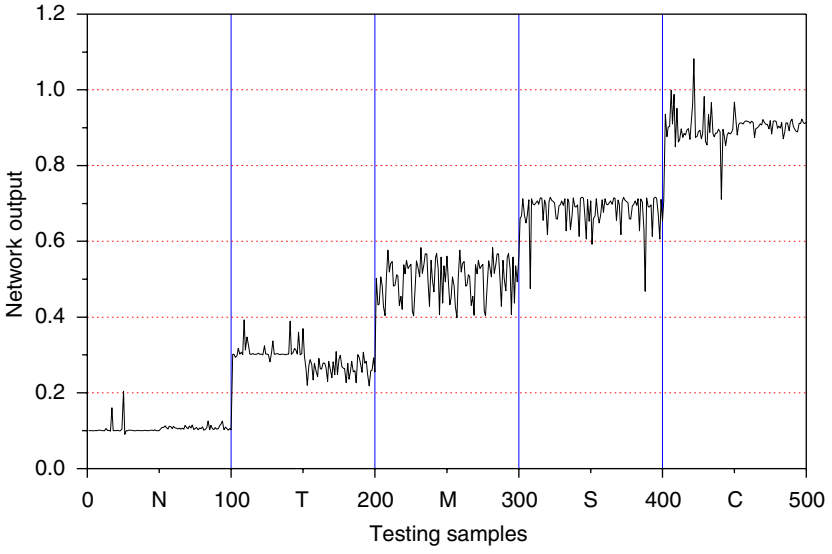

Fig. 14. Identification results by twofold-PCA method (30 PCs, $\sigma = 0.05$).

PCA methods, the identification accuracy in the case of high noise level is almost same as that in the case of low noise level. This demonstrates again the function of PCA as a noise filter. The twofold-PCA method achieves identification accuracy over 98% for both low and high noise cases.

Table 3
Number of correct identification times and IA for overall damage assessment

Damage case	Direct FRF method n (with $\sigma = 0.05$)		Once-PCA method σ (using 13 PCs)		Twofold-PCA method σ (using 30 PCs)	
	30	13	0.01	0.05	0.01	0.05
N	82 (100)	65 (100)	97 (100)	93 (100)	100 (100)	100 (100)
T	72 (100)	54 (100)	87 (100)	88 (100)	100 (100)	99 (100)
M	21 (100)	18 (100)	91 (100)	90 (100)	99 (100)	98 (100)
S	68 (100)	43 (100)	87 (100)	85 (100)	98 (100)	97 (100)
C	82 (100)	56 (100)	99 (100)	97 (100)	97 (100)	97 (100)
Σ	325 (500)	236 (500)	461 (500)	453 (500)	494 (500)	491 (500)
IA (%)	65.00	47.20	92.20	90.60	98.80	98.20

5.2. *Identification of damage location and distribution*

For damage location and distribution identification, a total of nine neural networks are configured with the same architecture as used for overall damage assessment. The 13 principal component projections extracted from each of nine FRFs are not grouped with each other. Instead, they are separately used as input to the nine neural networks. Accordingly, the damage at floors near a certain measurement point can be indicated by output of the respective network. All the nine neural networks are trained by using measurement data of the healthy structure, with the target output being the baseline value 0.1 for no damage case. With such trained neural networks, it is expected that the more damage occurs near a certain measurement point, the farer output of the respective network deviates from the baseline value. A damage index DI_i is thus defined, for the ith ($i = 1, 2, 3, 4$) damage case, as percentage deviation of the predicted output relative to the baseline value:

$$\mathrm{DI}_i = \frac{O_{\mathrm{di}} - 0.1}{0.1} \times 100\%, \tag{8}$$

where O_{di} is the output of neural network in the testing phase, 0.1 is the baseline value of no damage case. Thereafter, the damage location and distribution under a specific damage case can be indicated by the values of O_{di} from nine measurement points. The higher O_{di} of a certain floor, the more damage occurs near that location.

A total of 2700 samples from the nine measurement points (300 for each location) are generated for damage detection testing. Fig. 15 shows the DI_1 value for trifling damage case. It is seen that most of DI_1's are about 1%. Some fluctuation in the diagram is attributed to neural network training error, which is also the situation for other damage cases. Small value of DI_1 at all locations is due to the fact that in this case only minor damage occurs at a few columns around the transfer plate. Fig. 16 shows the DI_2 value for moderate damage case. It is seen that the DI_2 value below the 38th floor has an obvious deviation from the corresponding DI_1 value for trifling damage case, especially at 4th–10th floors. It implies that after moderate earthquake attack, considerable damage has been developed at the bottom portion from 4th to 10th floors. Fig. 17

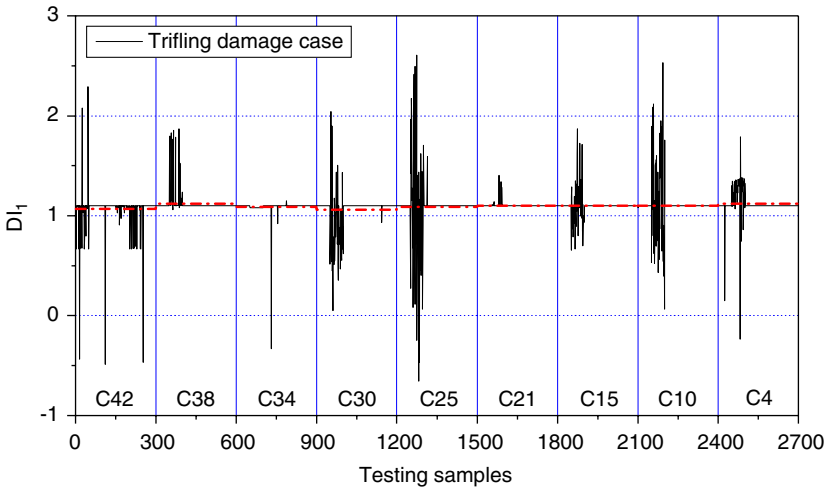

Fig. 15. Damage index sequence in trifling damage case.

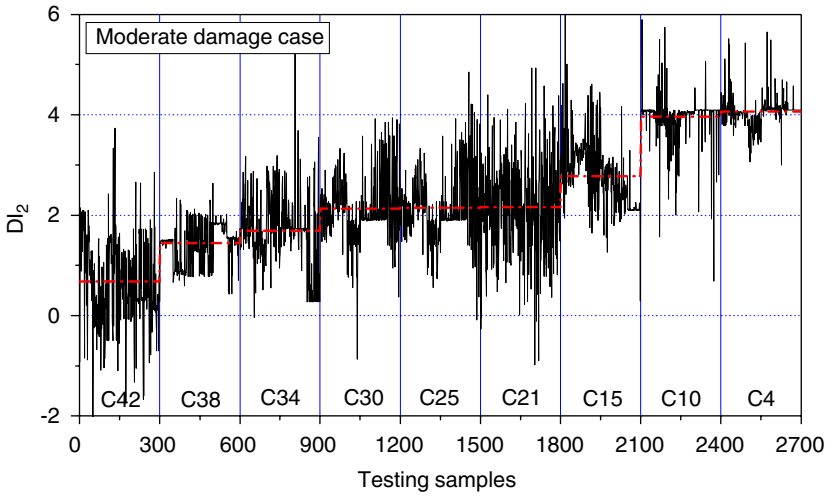

Fig. 16. Damage index sequence in moderate damage case.

shows the DI_3 value for serious damage case. The value of DI_3 at 15th–34th floors has a great increase in comparison with the corresponding value of DI_2, indicating that severe damage has occurred at middle and upper stories after strong earthquake excitation. Fig. 18 shows the DI_4 value for complete damage case. Extremely large value of DI_4 is found at 4th–15th floors, which agrees with the observation that during super-strong earthquake excitation the damage at the bottom portion extended dramatically to make the structure nearly collapsed and completely unrepairable. In each damage case, the average value of 300 DI_i's corresponding to one location has also been calculated to define a 'damage distribution profile', as plotted with dashed lines in the above figures. As a whole, the identified 'damage distribution profile' coincides fairly well with the visual inspection results of damage.

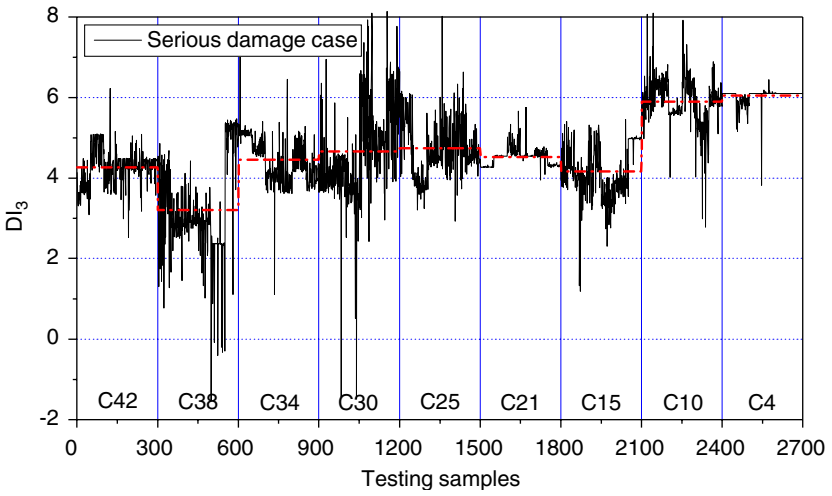

Fig. 17. Damage index sequence in serious damage case.

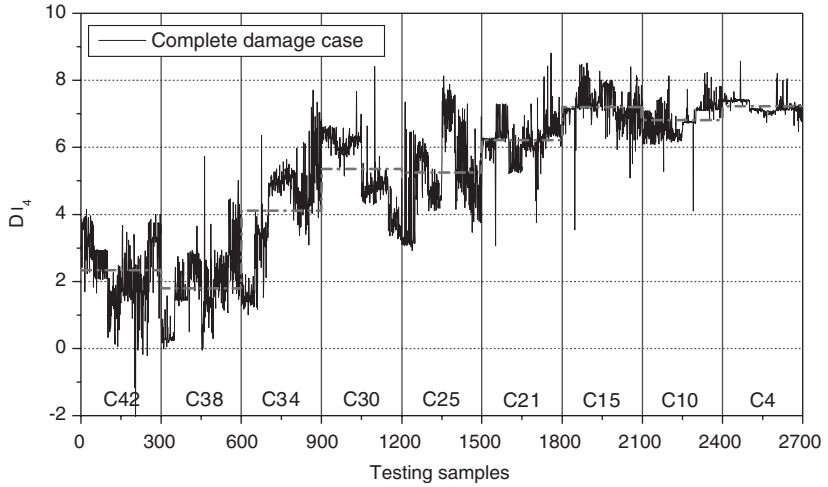

Fig. 18. Damage index sequence in complete damage case.

6. Conclusions

An experimental investigation has been conducted to examine the combined FRF and NN technique for seismic damage identification of tall building structures. The 38-storey model structure was tested to subject to four levels of earthquake action corresponding to minor, moderate, strong and super-strong earthquakes. After experiencing each level of earthquakes, low-intensity white-noise random excitation, which imitates post-earthquake ambient vibration monitoring, was exerted on the structure for the measurement of FRFs. PCA was then pursued to

reduce the dimensionality of FRF data by extracting essential features and disregarding unwanted measurement noise, which provided a better alternative for neural network implementation based on FRFs. Different NN architectures have been configured for both overall damage evaluation and damage location (distribution) identification of the tested structure. The following conclusions are drawn from this experimental study: (i) PCA is a powerful tool for reducing the size of measured FRF data. Even when a relatively small number of principal components are used, the PCA-compressed FRFs appear to account for most of the original information. (ii) A limited number of principal components retain prevailing features of the original FRFs, while filtering most of unwanted measurement noise. As a result, the reconstructed FRFs and subsequent damage identification results based on these few principal components are insensitive to noise. (iii) Compared with the direct FRF method, PCA methods provide much higher identification accuracy in damage assessment. Especially, the twofold-PCA method which utilizes information from different sensors is able to afford an accurate assessment of overall seismic damage. (iv) When sufficient sensors are distributed along the structure, the proposed method can offer a satisfactory evaluation of damage location. On the whole, the seismic damage distribution predicted by the proposed damage index is quite agreeable with the visual inspection results.

Acknowledgements

The work presented in this paper was supported by The Hong Kong Polytechnic University under the grant G-V856 and through the Area of Strategic Development Programme (Research Centre for Urban Hazards Mitigation). These supports are gratefully acknowledged.

References

[1] S.W. Doebling, C.R. Farrar, M.B. Prime, D.W. Shevitz, Damage identification and health monitoring of structural and mechanical systems from changes in their vibration characteristics: a literature review, Report No. LA-13070-MS, Los Alamos National Laboratory, Los Alamos, 1996.

[2] H. Sohn, C.R. Farrar, F.M. Hemez, D.D. Shunk, D.W. Stinemates, B.R. Nadler, J.J. Czarnecki, A review of structural health monitoring literature: 1996–2001, Report No. LA-13976-MS, Los Alamos National Laboratory, Los Alamos, 2004.

[3] N. Roitman, P.E. Viero, C. Magluta, R.C. Batista, L.F.L. Rosa, Identification of offshore platform structural damage using modal analysis techniques, *Mechanical Systems and Signal Processing* 6 (1992) 287–295.

[4] J.-S. Lew, Using transfer function parameter changes for damage detection of structures, *AIAA Journal* 33 (1995) 2189–2193.

[5] Z. Wang, R.M. Lin, M.K. Lim, Structural damage detection using measured FRF data, *Computer Methods in Applied Mechanics and Engineering* 147 (1997) 187–197.

[6] G.H. James III, D.C. Zimmerman, R.L. Mayes, Experimental study of frequency response function (FRF) based damage assessment tools, *Proceedings of the 16th International Modal Analysis Conference*, Santa Barbara, CA, 1998, pp. 151–157.

[7] S.K. Thyagarajan, M.J. Schulz, P.F. Pai, J. Chung, Detecting structural damage using frequency response functions, *Journal of Sound and Vibration* 210 (1998) 162–170.

[8] R.P.C. Sampaio, N.M.M. Maia, J.M.M. Silva, Damage detection using the frequency-response-function curvature method, *Journal of Sound and Vibration* 226 (1999) 1029–1042.

[9] U. Lee, J. Shin, A frequency response function-based structural damage identification method, *Computers and Structures* 80 (2002) 117–132.
[10] J.A. Pereira, W. Heylen, S. Lammens, P. Sas, Influence of the number of frequency points and resonance frequencies on model updating techniques for health condition monitoring and damage detection of flexible structure, *Proceedings of the 13th International Modal Analysis Conference*, Nashville, 1995, pp. 1273–1281.
[11] X. Wu, J. Ghaboussi, J.H. Garrett, Use of neural network in detection of structural damage, *Computers and Structures* 42 (1992) 649–659.
[12] Z. Chaudhry, A.J. Ganino, Damage detection using neural networks: an initial experimental study on debonded beams, *Journal of Intelligent Material Systems and Structures* 5 (1994) 585–589.
[13] R.-A. Manning, Structural damage detection using active members and neural networks, *AIAA Journal* 32 (1994) 1331–1333.
[14] J. Rhim, S.W. Lee, A neural network approach for damage detection and identification of structures, *Computational Mechanics* 16 (1995) 437–443.
[15] H. Luo, S. Hanagud, Dynamic learning rate neural training and composite structural damage detection, *AIAA Journal* 35 (1997) 1522–1527.
[16] S.-P. Chang, J. Lee, S. Kim, Damage detection in steel bridge using artificial neural network and signal anomaly index, in: D.L. Balageas (Ed.), *Structural Health Monitoring 2002*, DEStech Publications, Lancaster, PA, 2002, pp. 718–725.
[17] C. Zang, M. Imregun, Combined neural network and reduced FRF techniques for slight damage detection using measured response data, *Archive of Applied Mechanics* 71 (2001) 525–536.
[18] C. Zang, M. Imregun, Structural damage detection using artificial neural networks and measured FRF data reduced via principal component projection, *Journal of Sound and Vibration* 242 (2001) 813–827.
[19] I.T. Jolliffe, *Principal Component Analysis*, Springer, New York, 1986.
[20] G.H. Dunteman, *Principal Components Analysis*, Sage Publications, London, 1989.
[21] S.S.E. Lam, C.S. Li, M.Z. Zhang, Y.L. Wong, K.T. Chau, Seismic study of Hong Kong: shaking table tests of a typical high-rise building in Hong Kong, Research Report, Department of Civil and Structural Engineering, The Hong Kong Polytechnic University, Hong Kong, 2002.
[22] M.F. Elkordy, K.C. Chang, G.C. Lee, A structural damage neural network monitoring system, *Microcomputers in Civil Engineering* 9 (1994) 83–96.